Energy Fuels **2009,** *23,* 5886–5898 · DOI:10.1021/ef900726j
Published on Web 11/24/2009

energy&fuels
article

A Shock Tube Study of *n*- and *iso*-Propanol Ignition

Michael V. Johnson and S. Scott Goldsborough*

Department of Mechanical Engineering, Marquette University, Milwaukee, Wisconsin 53201-1881

Zeynep Serinyel, Peter O'Toole, Eoin Larkin, Grainne O'Malley, and Henry J. Curran

Combustion Chemistry Centre, National University of Ireland Galway, Galway, Ireland

Received July 13, 2009. Revised Manuscript Received October 22, 2009

An understanding of the ignition and oxidation characteristics of propanol, as well as other alcohols, is important toward the development and design of combustion engines that can effectively utilize bioderived and bioblended fuels. Building upon a database for "first-generation" alcohols including methanol and ethanol, the ignition characteristics of the two isomers of propanol (*n*-propanol and *iso*-propanol) have been studied in a shock tube. Ignition delay times for propanol/oxygen/argon mixtures have been measured behind reflected shock waves at temperatures ranging from approximately 1350 to 2000 K and a pressure of 1 atm. Equivalence ratios of 0.5, 1.0, and 2.0 have been used. Pressure measurements and CH* emissions were used to determine ignition delay times. The influences of equivalence ratio, temperature, and mixture strength on ignition delay have been characterized and compared to the behavior seen with a newly developed detailed kinetic mechanism. The overall trends are captured fairly well by the mechanism, which include a greater level of reactivity for the *n*-propanol mixtures relative to *iso*-propanol at the conditions used in this study.

1. Introduction

Interest in oxygenated fuels has increased significantly in recent years due to the needs to reduce emissions from combustion engines and to address climate change issues. Oxygenated fuels, which include ethers, esters, and alcohols, can be used as alternative fuel substitutes, or as fuel additives that can inhibit the formation of polyaromatic hydrocarbons (PAH) and soot, and improve ignition quality and combustion performance. If produced from biobased renewable sources, these oxygenated fuels have the potential to help balance emissions of carbon dioxide, a major greenhouse gas.

Low molecular weight alcohols, sometimes referred to as "first-generation" (1st-gen) alcohol fuels, including methanol (MeOH) and ethanol (EtOH), have been used widely in vehicular applications to address emissions problems in cold weather operation and as octane enhancers to improve overall engine performance. Recently, these have also been used as additives for engines employing low temperature combustion schemes such as homogeneous charge compression ignition (HCCI) in order to modulate ignition timing and heat release rates.[1,2] Numerous examples of uses of these fuels can be found throughout the SAE technical literature. A range of fundamental data have also been collected for these 1st-gen alcohols, including in shock tubes (ST), flow reactors, and others,[3−15] and detailed chemical mechanisms for these fuels, which are useful for the design of well performing engines, have been extensively developed covering a wide range of engine operating conditions.[16−18]

Significantly less work, however, has been devoted to higher molecular weight (MW) alcohols. These, sometimes referred to as "next-generation" alcohols, such as butanol (BuOH), pentanol (PeOH), etc., have benefits relative to MeOH and EtOH, including greater energy density, reduced evaporative emissions due to their lower vapor pressures, lower hygroscopicity, and reduced corrosiveness to materials used in fuel systems. Experimental studies using blends of gasoline and higher MW alcohols in spark-ignition engines have investigated effects on in-cylinder evaporation rates, knock-limits, burn rates, indicated mean effective pressure,

*To whom correspondence should be addressed. Telephone: 001-414-288-6641. Fax: 001-414-288-7790. E-mail: scott.goldsborough@mu.edu.

(1) Lu, X.; Ji., L.; Zu, L.; Huang, Z. *SAE Paper 2007−01−1875*, 2007.
(2) Kim, Y.-J.; Kim, K.-B.; Lee, K.-H. *SAE Paper 2008−32−0026*, 2008.
(3) Bowman, C. T. *Combust. Flame* **1975**, *25*, 343–354.
(4) Natarjan, K.; Bhaskaran, K. A. *Combust. Flame* **1981**, *43*, 35–49.
(5) Tsuboi, T.; Hashimoto, K. *Combust. Flame* **1981**, *42*, 61–76.
(6) Dunphy, M. P.; Simmie, J. M. *Combust. Flame* **1991**, *85*, 489–498.
(7) Cribb, P. H.; Dove, J. E.; Yamazaki, S. *Combust. Flame* **1992**, *88*, 186–200.
(8) Fieweger, K.; Blumenthal, R.; Adomeit, G. *Combust. Flame* **1997**, *109*, 599–619.
(9) Held, T. J.; Dryer, F. L. *Int. J. Chem. Kinet.* **1998**, *30*, 805–830.
(10) Shin, K. S.; Bae, G. T.; Yoo, S. J. *J. Korean Chem. Soc.* **2004**, *48*, 99–102.
(11) Nararajan, K.; Bhaskaran, K. A. *Thirteenth International Shock Tube Symposium*, Niagara Falls, 1981; pp 834−842.
(12) Dunphy, M. P.; Simmie, J. M. *J. Chem. Soc. Faraday Trans.* **1991**, *87*, 1691–1696.
(13) Curran, H. J.; Dunphy, M. P.; Simmie, J. M.; Westbrook, C. K.; Pitz, W. J. *Symp. (Int.) Combust.* **1992**, 769–776.
(14) Tsang, W. *Int. J. Chem. Kinet.* **2004**, *36*, 456–465.
(15) Shin, K. S.; Park, K. S.; Kwon, E. S. *J. Korean Chem. Soc.* **2004**, *48*, 12–16.
(16) Marinov, N. M. *Int. J. Chem. Kinet.* **1999**, *31*, 183–220.
(17) Li, J.; Kazakov, A.; Dryer, F. L. *Int. Chem. Kin.* **2001**, *33*, 859–867.
(18) Li, J.; Zhao, Z.; Kazakov, A.; Chaos, M.; Dryer, F. L.; Scire, J. J., Jr. *Int. J. Chem. Kinet.* **2007**, *39*, 109–136.

and thermal efficiency.[19−24] Studies with diesel/alcohol blends in direct-injection engines have investigated influences on ignition quality, power output, exhaust gas emissions, and fuel consumption.[25−27] Propanol (PrOH) blends with n-heptane have been studied in an HCCI engine to understand the influence on heat release timing/rate and emissions.[28] Fundamental investigations with BuOH in well controlled apparatuses have utilized low-pressure laminar flames,[29] shock tubes,[30,31] and jet stirred reactors.[32]

As next-generation alcohols are utilized in greater amounts there is a need to fundamentally understand their combustion chemistry, including the fuel's overall reactivity at engine-relevant conditions, as well as the chemical pathways responsible for PAH and soot reduction and the production of toxic oxygenated byproducts such as aldehydes. Hierarchically developed kinetic mechanisms employing base chemistry for small hydrocarbon molecules and submechanisms for larger, fuel-related species can be used to simulate relevant processes; reduced versions can be employed in coupled computational fluid dynamics analyses of new engine configurations and operating schemes. Ignition delay data from shock tube facilities are important targets for the development of these mechanisms as they elucidate the global reactivity of the fuel at various mixture strengths, temperatures, and pressures. Recent developments of in situ ST diagnostics are also enabling the quantification of fuel concentration and important intermediates such as OH during the rapid fuel decomposition and ignition processes.[33] Shock tubes have the advantage over other experimental techniques of being able to use engine-relevant conditions, including high pressures, and some have been designed for undiluted operation.[34]

The focus of this work is on propanol, a three-carbon alcohol that, while not considered as a next-gen alcohol itself, proceeds through decomposition/oxidation steps that are relevant to the oxidation and ignition of higher MW alcohols. Fundamental work to date with propanol includes the following studies. Norton and Dryer[35] investigated the oxidation of C_1- to C_4- alcohols (including *n*- and *iso*-propanol, or 1- and 2-propanol, respectively) and methyl *tert*-butyl ether (MTBE) using a pressurized flow reactor. On the basis of bond energy analysis and comparison between similar fuel structures, they assumed dehydrogenation and dehydration as possible decomposition channels. Sinha and Thomson[36] studied diffusion flames of C_3- oxygenated hydrocarbons and their mixtures, including *iso*-propanol, dimethoxy methane, and dimethyl carbonate. They concluded that the intermediate pools in their flames were strongly related to the fuel structural features. Bui et al.[37] conducted a theoretical investigation of *iso*-propanol pyrolysis under very low and high pressures to understand its unimolecular decomposition pathways. Li et al.[38] and Kasper et al.[39] have recently presented complementary isomer-specific intermediate species data, including several radicals in very low pressure ($p \sim 0.04$ atm) burner stabilized propanol and acetone flames. They used synchrotron photoionization and electron ionization molecular-beam mass spectrometry (MBMS) to unambiguously detect new flame species including propenols, butenols, and 1,3,5-hexatriyne. They noted that the differences between the isomeric flames were most pronounced for oxygenated intermediates formed directly from the fuel; their fuel-rich flames indicated a greater level of reactivity for *n*-propanol relative to *iso*-propanol at the low pressure, high oxygen concentration ($\chi_{O_2} \sim 50\%$) conditions (also Li and Qi[40]). Finally, Wang and Cadman[41] investigated PAH and soot production from spray combustion of *n*-propanol behind reflected shock waves.

The objective of this work is to build upon the growing fundamental database for next-generation alcohol fuels; here we present new ignition delay data for homogeneous shock tube experiments with the two isomers of propanol (*n*- and *iso*-propanol) and simulation results using a new detailed kinetic mechanism that has been developed for these isomers. Agreements and differences between the behavior seen in the shock tube experiments and that observed in the simulations are highlighted. As this mechanism is tested against additional data sets and further refined, it can be extended to increasingly heavier alcohol fuels, as has been done with heavier hydrocarbons (e.g., see refs 42 and 43).

The remainder of this paper is organized as follows. First the methods used in the shock tube experiments are described, followed by a discussion of the kinetic model. The results of the experiments are then presented along with analyses based on the model. Reaction flux and sensitivity analyses are discussed as well as correlations of the experimental data and simulated data points. Trends seen in the data and the model are highlighted, and these are compared to behavior of *n*- and *iso*-butane, two isomers of a saturated hydrocarbon with molecular structures similar to *n*- and *iso*-propanol,

(19) Bata, R. M.; Elrod, A. C.; Lewandowski, T. P. *SAE Paper 890434*, 1989.
(20) Popuri, S. S. S.; Bata, R. M. *SAE Paper 932953*, 1993.
(21) Saeengbangpla, P. *SAE Paper 958426*, 1995.
(22) Taylor, A. B.; Mocan, D. P.; Bell, A. J.; Hodgson, N. G.; Myburgh, I. S.; Botha, J. J. *SAE Paper 961988*, 1996.
(23) Gautam, M.; Martin, D. W. *Proc. Inst. Mech. Eng. Part A. J. Power Energy* **2000**, *214*, 497–511.
(24) Smith, J. D.; Sick, V. *SAE Paper 2007−01−4034*, 2007.
(25) Shirvani, H.; Goering, C. E.; Sorenson, S. C. *SAE Paper 810681*, 1981.
(26) Myburgh, I. S. *SAE Paper 861583*, 1986.
(27) Miers, S. A.; Carlson, R. W.; McConnell, S. S.; Ng, H. K.; Wallner, T.; LeFeber, J. *SAE Paper 2008−01−2381*, 2008.
(28) Xingcai, L.; Yuchun, H.; Libin, J.; Linlin, Z.; Zhen, H. *Energy Fuels* **2006**, *20*, 1870–1878.
(29) Yang, B.; Osswald, P.; Li, Y.; Wang, J.; Wei, L.; Tian, Z.; Qi, F.; Kohse-Höinghaus, K. *Combust. Flame* **2007**, *148*, 198–209.
(30) Zhukov, V.; Simmie, J.; Curran, H.; Black, G.; Pichon, S. Autoignition of Biobutanol. *21st Int. Conf. Dyn. Exp. Reactive Sys. (ICDERS)*, Poitiers, France, July 23−27, 2007.
(31) Moss, J. T.; Berkowitz, A. M.; Oehlschlaeger, M. A.; Biet, J.; Warth, V.; Glaude, P.-A.; Battin-Leclerc, F. *J. Phys. Chem. A.* **2008**, *112*, 10843–10855.
(32) Sarathy, S. M.; Thomson, M. J.; Tobgé, C.; Dagaut, P.; Halter, F.; Mounaim-Rousselle, C. *Combust. Flame* **2009**, *156*, 852–864.
(33) Vasu, S. S.; Davidson, D. F.; Hanson, R. K. *Combust. Flame* **2009**, *156*, 736–749.
(34) Aul, C. J.; Petersen, E. L., *Proc. 6th US Combust. Meeting*, Ann Arbor, MI, May 17-20, 2009; The Combustion Institute: Pittsburg, PA, 2009.
(35) Norton, T. S.; Dryer, F. L. *Proc. Combust. Inst.* **1991**, *23*, 179–185.
(36) Sinha, A.; Thomson, M. J. *Combust. Flame* **2004**, *136*, 548–556.
(37) Bui, B. H.; Zhu, R. S.; Lin, M. C. *J. Chem. Phys.* **2002**, *117*, 11188–11195.
(38) Li, Y.; Wei, L.; Tian, Z.; Yang, B.; Wang, J.; Zhang, T.; Qi, F. *Combust. Flame* **2008**, *152*, 336–359.
(39) Kasper, T.; O-wald, P.; Struckmeier, U.; Kohse-Höinghaus, K.; Taatjes, C. A.; Wang, J.; Cool, T. A.; Law, M. E.; Morel, A.; Westmoreland, P. R. *Combust. Flame* **2009**, *156*, 1181–1201.
(40) Li, Y.; Qi, F., National Synchrotron Radiation Laboratory, University of Science and Technology of China, personal communication, 2009.
(41) Wang, R.; Cadman, P. *Combust. Flame* **1998**, *112*, 359–370.
(42) Curran, H. J.; Gaffuri, P.; Pitz, W. J.; Westbrook, C. K. *Combust. Flame* **1998**, *114*, 149–177.
(43) Westbrook, C. K.; Pitz, W. J.; Herbinet, O.; Curran, H. J.; Silke, E. J. *Combust. Flame* **2009**, *256*, 181–199.

respectively, where a methyl group is substituted for the hydroxyl group. At the conclusion, the findings of this study are summarized, along with additional steps to be taken in the mechanism development.

2. Experimental Section

The experiments were conducted in the low pressure, stainless steel shock tube facility at the National University of Ireland Galway's Combustion Chemistry Centre. The facility has been reported elsewhere,[44,45] but a brief description is provided here. The ST consists of three main sections: a high volume driver section, 52 cm diameter by 63 cm long; a transition section that is 10 cm long; and a test section measuring 10.24 cm in diameter by 622 cm long. The test and transition sections are separated by a single polycarbonate burst diaphragm. The diaphragm is burst using a stationary mechanical cutter as the driver section is pressurized with helium (99.99% pure, BOC). The diaphragm separates into four petals upon rupture, minimizing the formation of small diaphragm particles that can contaminate the test section. Diaphragm thickness can be varied to achieve different strength shock waves; the target pressure for this study was 1 atm.

Reactant mixtures are made externally to the shock tube in a 50 L stainless steel mixing vessel that is initially evacuated to 1×10^{-6} torr. Fuel and oxygen are added using the method of partial pressures with measurements made using a high-accuracy (±0.01 torr) Baratron pressure manometer (100 torr full scale). The balance of the mixture is made with argon to a pressure of 800 torr, with this measured by a Chell CD101 manometer (900 torr full scale). The mixture is allowed to sit for a minimum of 1 h before use. The oxygen (99.5% pure) and argon (99.9% pure) were purchased from BOC. The propanol (*n*-propanol +99% spectro-photometric grade; *iso*-propanol +99.5% ACS reagent grade) was purchased from Sigma Aldrich. *n*-Propanol has a vapor pressure of 16.73 torr at 22 °C, and that of iso-propanol is 35.26 torr at the same temperature. The highest partial pressure of fuel used was 4 torr, which is well below the vapor pressure limit; consequently, it is highly unlikely that there is any adsorption of either fuel on the walls of the mixing tank or shock tube. The propanol isomers were degassed using a series of freeze−pump−thaw cycles with liquid nitrogen, after which no more gas was observed to escape on thawing the solid. The test mixtures are delivered to the shock tube after the test section and driver section have been evacuated to pressures of 1×10^{-6}, and 1×10^{-3} torr, respectively, using Edwards high vacuum pumps, models E2M8 and E1M8, respectively. The test section is charged to an initial pressure of 15−30 torr, and the driver section is then filled with helium until the diaphragm bursts. Each experiment is carried out such that the fuel mixture resides in the driven section of the tube for no more than 2−3 minutes.

The shock tube is equipped with four piezoelectric pressure transducers (PCB transducer model 113A21) with rise times of ≤1 μs spaced over the last 50 cm of the test section for measurement of the incident shock velocity. The transducers are flush mounted in the shock tube sidewall and the signals are sent to universal time counters (Fluke PM6666) that provide the time intervals for incident shock passage, allowing determination of the incident shock wave velocities at three locations over the last 150 cm of the test section. The three incident shock velocities are linearly extrapolated to the shock tube endwall to determine the incident shock velocity at the test section.

The incident and reflected shock conditions (vibrationally equilibrated) are calculated by using the normal shock relations in the software GasEQ.[46] The measured incident shock velocity at the test location, the measured initial temperature and pressure, and the thermodynamic properties of the reactant mixture are inputs to the calculations. The initial temperature is measured by using a mercury thermometer, and the initial pressure is measured by using another high-accuracy (±0.01 torr) Baratron pressure manometer (100 torr full scale). The thermodynamic data for both propanol isomers were calculated using the THERM program of Ritter and Bozzelli,[47] based on group additivity methods developed by Benson.[48] These data are in agreement with estimates in the NIST WebBook[49] and with the Burcat and Ruscic database.[50] The bond dissociation energies for *n*-propanol and *iso*-propanol are reported in Figures 1 and 2, respectively; and for *n*-propanol the values agree well with those that we have reported for *n*-butanol.[45]

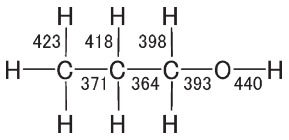

Figure 1. Bond dissociation energies of *n*-propanol (kJ mol^{-1}).

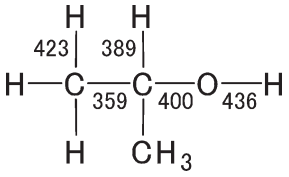

Figure 2. Bond dissociation energies of *iso*-propanol (kJ mol^{-1}).

Experimental ignition delay times (τ) are defined as the time interval between shock arrival and reflection at the endwall, and the onset of ignition. The shock arrival and reflection is measured using a Kistler 603B piezoelectric transducer mounted flush in the endwall. The onset of ignition was determined based on the 50% rise point of the emission from electronically excited CH radicals (CH*). The CH* emission is observed through a fused silica window mounted in the shock tube endwall. The CH* emission is separated from other optical interference by using a 431.5 nm narrow bandpass filter with a 10 nm spectral bandwidth and recorded with a Thorlabs PDA55 silicon photodetector. The pressure transducer and emission signals were recorded using a Tekronix TDS 2024 oscilloscope. See Figure 3 for an example ignition time measurement.

Prior to performing measurements for propanol, ignition delay time measurements were taken for *n*-heptane behind reflected shock waves at the conditions of previous shock tube studies that have been published in the literature. This was done to validate the experimental techniques. The data from Smith et al.,[44] Horning et al.,[51] and Pichon et al.[52] were used to calibrate our *n*-heptane measurements based on our confidence in those data

(44) Smith, J. M.; Simmie, J. M.; Curran, H. J. *Int. J. Chem. Kinet.* **2005**, *37*, 728–736.
(45) Black, G.; Curran, H. J.; Pichon, S.; Simmie, J. M.; Zhukov, V. *Combust. Flame* **2009**, in press. (doi:10.1016/j.combustflame.2009.07.007).
(46) Morley, C. Gaseq: A Chemical Equilibrium Program for Windows, http://www.arcl02.dsl.pipex.com/.
(47) Ritter, E. R.; Bozzelli, J. W. *Int. J. Chem. Kinet.* **1991**, *23*, 767–778.
(48) Benson, S. W. *Thermochemical Kinetics*; John Wiley & Sons: New York, 1976.
(49) Stein, S. E. Brown, R. L., *Structures and Properties Group Additivity Model" in NIST Chemistry WebBook, NIST Standard Reference Database Number 69*; Linstrom, P.J., Mallard, W. G., Eds.; National Institute of Standards and Technology: Gaithersburg MD, 2005; http://webbook.nist.gov.
(50) Burcat, A.; Ruscic, B. *Ideal Gas Thermochemical Database with updates from Active Thermochemical Tables*: ftp://ftp.technion.ac.il/pub/supported/aetdd/thermodynamics; July 14, 2008.
(51) Horning, D. C.; Davidson, D. F.; Hanson, R. K. *J. Propulsion Power* **2002**, *18*, 363–371.
(52) Pichon, S.; Black, G.; Chaumeix, N.; Yahyaoui, M.; Simmie, J. M.; Curran, H. J.; Donohue, R. *Combust. Flame* **2009**, *156*, 494–504.

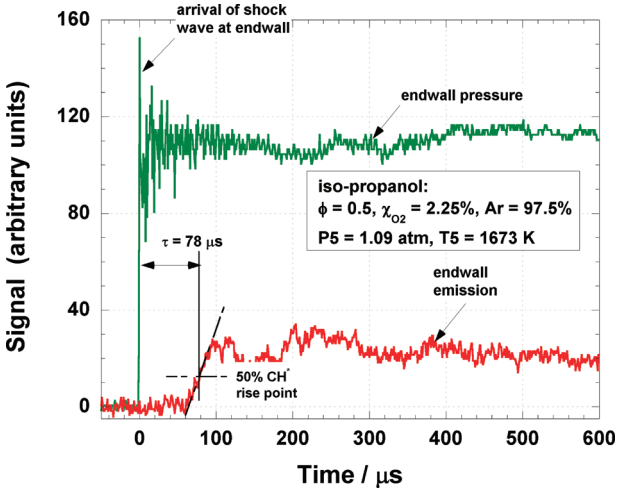

Figure 3. Example pressure and CH* signals for a typical shock tube experiment illustrating the definition of ignition delay time.

sets. The validation measurements are in excellent agreement with the previous studies.

3. Model

The propanol mechanism is based on the hierarchical structure of chemical kinetic mechanisms and uses our updated C3- chemistry[53] for the baseline chemistry, with the propanol isomer submechanisms added. These submechanisms were systematically generated considering (i) unimolecular fuel decomposition reactions, (ii) hydrogen atom abstraction reactions, and (iii) β-scission reactions associated with the alkyl/alkoxy radicals generated from the parent fuel.

Unimolecular Decomposition. The propanol submechanism includes the two possible classes of unimolecular decomposition reaction: simple and complex fission. According to our thermochemistry, the weakest bond in the molecule is the C_α—C_β bond, as would be expected given its proximity to the electron withdrawing hydroxyl group. This is consistent with the experimental findings of Barnard,[54] who proposes fission of this bond to be the primary decomposition pathway on the basis that formaldehyde is the predominant pyrolysis product observed, while other aldehydes and lower alcohols are absent. The remaining bond dissociation energies follow the order shown in Figures 1 and 2, and this is reflected in the fission rates, with breaking of the C−O and C−H bonds not competitive.

For the molecular elimination reactions, listed as reaction numbers 1329 and 1395 in the mechanism, rate constants are estimated based on Tsang's work[55] on the elimination of water from alkyl-substituted alcohols. For *n*-propanol (1329) a rate constant of $3.52 \times 10^{13}\ \exp(-33\,850/T)\ s^{-1}$ was estimated, and for *iso*-propanol (1395) a value of $2.11 \times 10^{14}\ \exp(-33\,850/T)\ s^{-1}$ was included, which are largely based on Tsang's recommendations for the elimination of water and 2,3-dimethylbut-1-ene and 2,4-dimethylbut-2-ene from 2,3-dimethylbutan-2-ol, respectively. The frequency factors were chosen to account for degeneracy of available hydrogen atoms possible in the transition state.

$$n\mathrm{CH_3CH_2CH_2OH} \xrightarrow{1329} \mathrm{C_3H_6} + \mathrm{H_2O}$$

$$i\mathrm{CH_3(CH_3)CHOH} \xrightarrow{1395} \mathrm{C_3H_6} + \mathrm{H_2O}$$

All of the other simple fission decomposition reactions were treated as bimolecular:

$$n\mathrm{CH_3CH_2CH_2OH} + \mathrm{M} \xrightarrow{1330} {}^{\bullet}\mathrm{CH_3} + {}^{\bullet}\mathrm{CH_2CH_2OH} + \mathrm{M}$$

$$n\mathrm{CH_3CH_2CH_2OH} + \mathrm{M} \xrightarrow{1331} {}^{\bullet}\mathrm{C_2H_5} + {}^{\bullet}\mathrm{CH_2OH} + \mathrm{M}$$

$$n\mathrm{CH_3CH_2CH_2OH} + \mathrm{M} \xrightarrow{1332} {}^{\bullet}n\mathrm{C_3H_7} + {}^{\bullet}\mathrm{OH} + \mathrm{M}$$

$$n\mathrm{CH_3CH_2CH_2OH} + \mathrm{M} \xrightarrow{1333} {}^{\bullet}3\mathrm{C_3H_6OH} + {}^{\bullet}\mathrm{H} + \mathrm{M}$$

$$n\mathrm{CH_3CH_2CH_2OH} + \mathrm{M} \xrightarrow{1334} {}^{\bullet}2\mathrm{C_3H_6OH} + {}^{\bullet}\mathrm{H} + \mathrm{M}$$

$$n\mathrm{CH_3CH_2CH_2OH} + \mathrm{M} \xrightarrow{1335} {}^{\bullet}1\mathrm{C_3H_6OH} + {}^{\bullet}\mathrm{H} + \mathrm{M}$$

$$n\mathrm{CH_3CH_2CH_2OH} + \mathrm{M} \xrightarrow{1336} n\mathrm{C_3H_7O}^{\bullet} + {}^{\bullet}\mathrm{H} + \mathrm{M}$$

$$i\mathrm{CH_3(CH_3)CHOH} + \mathrm{M} \xrightarrow{1396} {}^{\bullet}\mathrm{CH_3} + \mathrm{CH_3}{}^{\bullet}\mathrm{CHOH} + \mathrm{M}$$

$$i\mathrm{CH_3(CH_3)CHOH} + \mathrm{M} \xrightarrow{1397} {}^{\bullet}i\mathrm{C_3H_7} + {}^{\bullet}\mathrm{OH} + \mathrm{M}$$

The high-pressure limit rate constants for each of these reactions were calculated from microscopic reversibility using an estimate of the rate constant for the reverse, radical−radical recombination producing the fuel molecule. For reaction −1330 (i.e., the reverse of reaction 1330) a rate constant of $1.93 \times 10^{14}\ T^{-0.32}\ \mathrm{cm^3\ mol^{-1}\ s^{-1}}$, identical to that recommended by Tsang,[56] for methyl recombination with *n*-propyl radical was used, while for reaction −1331 a rate constant of approximately half of this was used. For reactions −1332 and −1397 a rate constant of $2.41 \times 10^{13}\ \mathrm{cm^3\ mol^{-1}\ s^{-1}}$ as recommended by Tsang[58] was used. For reaction −1396 a rate constant of $6.63 \times 10^{14}\ T^{-0.57}\ \mathrm{cm^3\ mol^{-1}\ s^{-1}}$ was estimated based on the recommendation of Tsang[57] for isopropyl and methyl radical recombination. Finally, for the reactions involving the recombination of a hydrogen atom with a C3- alkyl/alkoxy radical, a rate constant of $1.0 \times 10^{14}\ \mathrm{cm^3\ mol^{-1}\ s^{-1}}$ was used.

Thereafter, a chemical activation formulation based on quantum Rice−Ramsperger−Kassel theory, as described by Dean,[58,59] was then used together with the high-pressure limit expressions to develop pressure-dependent rate constants that were ultimately fit to a nine-parameter Troe formalism.[60]

Hydrogen Abstraction. Rate constants for hydrogen abstraction are based on those published recently for *n*-butanol oxidation.[45] Briefly, the rate constant for abstraction from the γ position relative to the OH group in *n*-propanol and for

(53) Bourque, G.; Healy, D.; Curran, H.; Zinner, C.; Kalitan, D.; de Vries, J.; Aul, C.; Petersen, E. *Proc. ASME Turbo Expo*. **2008**, *3*, 1051–1066.
(54) Barnard, J. A. *Trans. Faraday Soc*. **1957**, *53*, 1423–1430.
(55) Tsang, W. *Int. J. Chem. Kinet*. **1976**, *8*, 173–192.
(56) Tsang, W. *J. Phys. Chem. Ref. Data* **1988**, *17*, 887–952.
(57) Tsang, W. *Combust. Flame* **1989**, *78*, 71–86.
(58) Dean, A. M. *J. Phys. Chem*. **1985**, *89*, 4600–4608.
(59) Dean, A. M.; Bozzelli, J. M.; Ritter, E. R. *Combust. Sci. Technol*. **1991**, *80*, 63–85.
(60) Gilbert, R. G.; Luther, K.; Troe, J.; Bunsenges, Ber. *Phys. Chem*. **1983**, *87*, 169–177.
(61) Orme, J. P.; Curran, H. J.; Simmie, J. M. *J. Phys. Chem. A* **2006**, *110*, 114–131.

one of the six primary hydrogen atoms in *iso*-propanol is taken to be identical to that previously published for abstraction from a primary carbon in an alkane.[61] Abstractions at the α position and from the hydroxyl group were likened to the equivalent reactions in ethanol[62−64] for *n*-propanol, and in the case of the α position for *iso*-propanol the rate was increased by the same amount as it does in going from an α to a β hydrogen atom, since the bond dissociation energy change of 9 kJ mol^{-1} is about the same in both cases. As the hydrogen of the alcohol group is both the most tightly bound, and statistically the least likely to be abstracted, this pathway is not expected to be important, as observed by previous authors.[65] For abstraction from the β position we chose a rate constant identical to the β position in butanol, since the bond dissociation energies and local environment are virtually identical. In butanol this rate constant was estimated to be an average of the rate for abstraction of γ and δ hydrogen atoms.

Radical Decomposition. The alkyl/alkoxy radicals decompose primarily by β-scission:

$$^{\bullet}3C_3H_6OH \xrightarrow{1381} C_2H_4 + {}^{\bullet}CH_2OH$$

$$^{\bullet}2C_3H_6OH \xrightarrow{1382} C_3H_6 + {}^{\bullet}OH$$

$$^{\bullet}1C_3H_6OH \xrightarrow{1383} C_3H_3OH + {}^{\bullet}CH_3$$

$$^{\bullet}1C_3H_6OH \xrightarrow{1384} C_2H_5CHO + {}^{\bullet}H$$

$$^{\bullet}1C_3H_6OH \xrightarrow{1385} CH_3CH{=}CHOH + {}^{\bullet}H$$

$$nC_3H_7O^{\bullet} \xrightarrow{615} CH_2O + {}^{\bullet}C_2H_5$$

$$nC_3H_7O^{\bullet} \xrightarrow{616} C_2H_5CHO + {}^{\bullet}H$$

$$iC_3H_7O^{\bullet} \xrightarrow{617} CH_3CHO + {}^{\bullet}CH_3$$

$$iC_3H_7O^{\bullet} \xrightarrow{618} (CH_3)_2C{=}O + {}^{\bullet}H$$

$$^{\bullet}tC_3H_6OH \xrightarrow{1297} (CH_3)_2C{=}O + {}^{\bullet}H$$

$$^{\bullet}tC_3H_6OH \xrightarrow{1298} iC_3H_5OH + {}^{\bullet}H$$

$$^{\bullet}iC_3H_6OH \xrightarrow{1414} C_3H_6 + {}^{\bullet}OH$$

$$^{\bullet}iC_3H_6OH \xrightarrow{1415} C_2H_3OH + {}^{\bullet}CH_3$$

It is interesting to note that the decomposition of these radicals results in the formation of a number of different unsaturated alcohols—ethenol (C_2H_3OH), 1-propen-1-ol ($CH_3CH{=}CHOH$), and propen-2-ol (iC_3H_5OH). These enols are capable of tautomerising to form the corresponding aldehydes. However, in the gas phase these enolic species will be produced and so reactions involving their formation and consumption must be included together with their thermochemistry.

All rate constants for these reactions were estimated based on the work of Curran;[66] alkyl radical β-scission reactions are endothermic processes, thus this type/class of reaction is considered in the reverse, exothermic direction, the addition of a smaller alkyl/alkoxy radical to an olefin with the rate constant for the decomposition of the parent radical calculated using microscopic reversibility. Reactions 615−618 have already been published by Curran.[66] The rate constant for reaction −1381 was estimated to be $1.32 \times 10^4\ T^{2.48} \exp(-3085/T)$ $cm^3\ mol^{-1}\ s^{-1}$ as per the rate constant for an ethyl radical addition to ethylene recommended by Curran.[66] For reaction −1383 a rate constant of $1.76 \times 10^4\ T^{2.48} \exp(-3085/T)$ $cm^3\ mol^{-1}\ s^{-1}$ was used where this is analogous to that for methyl addition to propene forming the sec-butyl radical in the work of Curran.[66] Finally, for reaction −1415 a rate constant of $1.89 \times 10^3\ T^{2.67} \exp(-3450/T)$ $cm^3\ mol^{-1}\ s^{-1}$ was used, which is that recommended by Curran for methyl addition to propene forming the *iso*-butyl radical.

A rate constant of $9.93 \times 10^{11} \exp(483/T)$ $cm^3\ mol^{-1}\ s^{-1}$ was estimated for the addition of a hydroxyl radical to an olefinic species (reactions −1382 and −1414), with the rate constant for the decomposition of the alkyl radical calculated via microscopic reversibility. Reactions −616, −618, −1297, −1298, −1384, and −1385 all involve the elimination of a hydrogen atom with the generation of an aldehyde, ketone, or enolic species. Rate constants for the reverse addition of a hydrogen atom to the olefin are taken to be identical to those for hydrogen atom addition to ethylene and propene as provided in the work of Curran.[66] Reactions −1298 and −1385 involve the addition of a hydrogen atom to the oxygen atom in a C=O bond. The activation energy for this reaction was calculated by Simmie and Curran[67] to be 38 kJ mol^{-1}, with an estimated pre-exponential frequency factor of 8.0×10^{12} $cm^3\ mol^{-1}\ s^{-1}$. Some C−H bond breaking may be neglected in the case of $2C_3H_6OH$ and $3C_3H_6OH$. These reactions could play a minor role at high temperatures but we have not included them as C−C bond cleavage is expected to be faster up to the highest temperatures of our study.

A summary of the primary reaction rate constants is presented in Tables 1 and 2 for *n*- and *iso*-propanol, respectively. A full listing of the mechanism and thermochemistry can be found at: http://c3.nuigalway.ie/biofuels.html.

4. Simulations

The simulations conducted for this study utilize a homogeneous reactor model with constant volume/constant internal energy assumptions. Li et al.[68] have presented and discussed means to improve this approximation in order to account for nonideal gas dynamic effects, which can be especially important for high pressure, high mixture strength operation, and/or long test times. For some of the lower temperature experiments conducted here these effects may alter the measured delay times; more accurate comparisons

(62) Park, J.; Xu, Z. F.; Lin, M. C. *J. Chem. Phys.* **2003**, *188*, 9990–9996.
(63) Xu, Z. F.; Park, J.; Lin, M. C. *J. Chem. Phys.* **2004**, *120*, 6593–6599.
(64) Wu, C. W.; Lee, Y. P.; Xu, S.; Lin, M. C. *J. Phys. Chem. A* **2007**, *111*, 6693–6703.
(65) McEnally, C. S.; Pfefferle, L. D. *Proc. Combust. Inst.* **2005**, *30*, 1363–1370.
(66) Curran, H. J. *Int. J. Chem. Kinet.* **2006**, *38*, 250–275.
(67) Simmie, J. M.; Curran, H. J. *J. Phys. Chem. A* **2009**, *113*, 7834–7845.
(68) Li, H.; Owens, Z. C.; Davidson, D. F.; Hanson, R. K. *Int. J. Chem. Kinet.* **2008**, *40*, 189–198.

Table 1. Reaction Rate Constants for Unimolecular Decomposition and Hydrogen Abstraction Reactions for *n*-Propanol (cm mol s cal K units)

No.	reactions			*A*	*n*	E_a
1329	$nC_3H_7OH(+M)$	=	$C_3H_6 + H_2O(+M)$			
			high P limit	3.53×10^{13}	0.00	67260
			low P limit	1.99×10^{81}	−18.59	78190
			Troe parameters: $a = 0.13$	T3 = 1.0	T1 = 8.94×10^9	T2 = 9.33×10^9
1330	$nC_3H_7OH(+M)$	=	$CH_3 + pC_2H_4OH(+M)$			
			high P limit	8.81×10^{23}	−2.12	89 820
			low P limit	2.20×10^{64}	−13.39	95330
			Troe parameters: $a = 0.307$	T3 = 1110	T1 = 9.33×10^9	T2 = 9.33×10^9
1331	$nC_3H_7OH(+M)$	=	$C_2H_5 + CH_2OH(+M)$			
			high P limit	1.03×10^{24}	−2.20	88 260
			low P limit	1.45×10^{65}	−13.66	93 980
			Troe parameters: $a = 0.293$	T3 = 1102	T1 = 9.63×10^9	T2 = 9.33×10^9
1332	$nC_3H_7OH(+M)$	=	$nC_3H_7 + OH$			
			high P limit	5.26×10^{20}	−1.34	94 630
			low P limit	8.92×10^{57}	−11.78	99 410
			Troe parameters: $a = 0.355$	T3 = 942	T1 = 9.92×10^9	T2 = 9.92×10^9
1333	nC_3H_7OH	=	$3C_3H_6OH + H$	1.84×10^{17}	−0.36	101 200
1334	nC_3H_7OH	=	$2C_3H_6OH + H$	3.52×10^{18}	−0.73	100 400
1335	nC_3H_7OH	=	$1C_3H_6OH + H$	1.78×10^{16}	−0.17	95 310
1336	nC_3H_7OH	=	$nC_3H_7O + H$	7.03×10^{14}	0.07	104 900
1337	$nC_3H_7OH + O_2$	=	$3C_3H_6OH + HO_2$	3.00×10^{13}	0.00	52 290
1338	$nC_3H_7OH + O_2$	=	$2C_3H_6OH + HO_2$	2.44×10^{12}	0.22	49 760
1339	$nC_3H_7OH + O_2$	=	$1C_3H_6OH + HO_2$	2.00×10^{13}	0.00	49 460
1340	$nC_3H_7OH + O_2$	=	$nC_3H_7O + HO_2$	1.00×10^{13}	0.00	48 200
1341	$nC_3H_7OH + H$	=	$3C_3H_6OH + H_2$	6.66×10^5	2.54	6756
1342	$nC_3H_7OH + H$	=	$2C_3H_6OH + H_2$	1.11×10^5	2.40	2010
1343	$nC_3H_7OH + H$	=	$1C_3H_6OH + H_2$	1.79×10^5	2.53	3420
1344	$nC_3H_7OH + H$	=	$nC_3H_7O + H_2$	5.36×10^4	2.53	4405
1345	$nC_3H_7OH + OH$	=	$3C_3H_6OH + H_2O$	5.28×10^9	0.97	1586
1346	$nC_3H_7OH + OH$	=	$2C_3H_6OH + H_2O$	5.59×10^7	1.61	1176
1347	$nC_3H_7OH + OH$	=	$1C_3H_6OH + H_2O$	5.56×10^{10}	0.50	−380
1348	$nC_3H_7OH + OH$	=	$nC_3H_7O + H_2O$	1.50×10^{10}	0.80	2534
1349	$nC_3H_7OH + O$	=	$3C_3H_6OH + OH$	9.81×10^5	2.43	4750
1350	$nC_3H_7OH + O$	=	$2C_3H_6OH + OH$	1.44×10^5	2.61	3029
1351	$nC_3H_7OH + O$	=	$1C_3H_6OH + OH$	1.45×10^5	2.47	876
1352	$nC_3H_7OH + O$	=	$nC_3H_7O + OH$	1.58×10^7	2.00	4448
1353	$nC_3H_7OH + HO_2$	=	$3C_3H_6OH + H_2O_2$	2.38×10^4	2.55	16 490
1354	$nC_3H_7OH + HO_2$	=	$2C_3H_6OH + H_2O_2$	2.30×10^{-3}	3.37	466
1355	$nC_3H_7OH + HO_2$	=	$1C_3H_6OH + H_2O_2$	6.00×10^{12}	0.00	16 000
1356	$nC_3H_7OH + HO_2$	=	$nC_3H_7O + H_2O_2$	2.50×10^{12}	0.00	24 000
1357	$nC_3H_7OH + CH_3O_2$	=	$3C_3H_6OH + CH_3O_2H$	2.38×10^4	2.55	16 490
1358	$nC_3H_7OH + CH_3O_2$	=	$2C_3H_6OH + CH_3O_2H$	1.56×10^3	2.81	14 280
1359	$nC_3H_7OH + CH_3O_2$	=	$1C_3H_6OH + CH_3O_2H$	6.00×10^{12}	0.00	16 000
1360	$nC_3H_7OH + CH_3O_2$	=	$nC_3H_7O + CH_3O_2H$	2.50×10^{12}	0.00	24 000
1361	$nC_3H_7OH + CH_3$	=	$3C_3H_6OH + CH_4$	4.53×10^{-1}	3.65	7154
1362	$nC_3H_7OH + CH_3$	=	$2C_3H_6OH + CH_4$	8.02×10^0	3.23	6461
1363	$nC_3H_7OH + CH_3$	=	$1C_3H_6OH + CH_4$	1.99×10^1	3.37	7634
1364	$nC_3H_7OH + CH_3$	=	$nC_3H_7O + CH_4$	2.04×10^0	3.57	7721
1365	$nC_3H_7OH + C_2H_5$	=	$3C_3H_6OH + C_2H_6$	4.62×10^{-1}	3.65	9142
1366	$nC_3H_7OH + C_2H_5$	=	$2C_3H_6OH + C_2H_6$	7.66×10^0	3.11	12 210
1367	$nC_3H_7OH + C_2H_5$	=	$1C_3H_6OH + C_2H_6$	2.00×10^{11}	0.00	11 000
1368	$nC_3H_7OH + C_2H_5$	=	$nC_3H_7O + C_2H_6$	1.00×10^{11}	0.00	9200
1369	$nC_3H_7OH + HCO$	=	$3C_3H_6OH + CH_2O$	1.02×10^5	2.50	18 440
1370	$nC_3H_7OH + HCO$	=	$2C_3H_6OH + CH_2O$	5.16×10^5	2.25	16 760
1371	$nC_3H_7OH + HCO$	=	$1C_3H_6OH + CH_2O$	1.00×10^7	1.90	17 000
1372	$nC_3H_7OH + HCO$	=	$nC_3H_7O + CH_2O$	3.40×10^4	2.50	13 500
1373	$nC_3H_7OH + CH_2OH$	=	$3C_3H_6OH + CH_3OH$	1.01×10^2	2.95	13 970
1374	$nC_3H_7OH + CH_2OH$	=	$2C_3H_6OH + CH_3OH$	1.53×10^1	3.11	12 210
1375	$nC_3H_7OH + CH_2OH$	=	$1C_3H_6OH + CH_3OH$	6.00×10^1	2.95	12 000
1376	$nC_3H_7OH + CH_2OH$	=	$nC_3H_7O + CH_3OH$	1.20×10^2	2.76	10 800
1377	$nC_3H_7OH + CH_3O$	=	$3C_3H_6OH + CH_3OH$	2.17×10^{11}	0.00	6458
1378	$nC_3H_7OH + CH_3O$	=	$2C_3H_6OH + CH_3OH$	3.02×10^0	0.18	4703
1379	$nC_3H_7OH + CH_3O$	=	$1C_3H_6OH + CH_3OH$	1.50×10^0	2.95	4500
1380	$nC_3H_7OH + CH_3O$	=	$nC_3H_7O + CH_3OH$	2.30×10^{10}	0.00	2900
1381	$3C_3H_6OH$	=	$C_2H_4 + CH_2OH$	1.54×10^{11}	0.83	28 660
1382	$2C_3H_6OH$	=	$C_3H_6 + OH$	5.09×10^{15}	−0.95	26 260
1383	$1C_3H_6OH$	=	$C_2H_3OH + CH_3$	5.01×10^{10}	1.04	30 450
1384	$1C_3H_6OH$	=	$C_2H_5CHO + H$	7.04×10^9	0.99	32 590
1385	$1C_3H_6OH$	=	$CH_3CHCHOH + H$	5.46×10^{11}	0.34	35 630

between the experiments and simulations could take these nonideal effects into account.

HCT,[69] the chemical kinetics solver developed by Lawrence Livermore National Laboratory (LLNL), was used to perform the calculations. Since CH* is not included in the propanol mechanism, the computed ignition delay times are based on peak values of $[C_2H] \times [O]$ ($\tau_{C_2H_xO,peak}$). Times computed in this manner are slightly longer than if based on

Table 2. Reaction Rate Constants for Unimolecular Decomposition and Hydrogen Abstraction Reactions for *iso*-Propanol (cm mol s cal K units)

No.	reactions			A	n	E_a
1395	$iC_3H_7OH(+M)$	=	$C_3H_6 + H_2O(+M)$			
			high P limit	2.11×10^{14}	0.00	67 260
			low P limit	3.61×10^{82}	−18.85	79 340
			Troe parameters: $a = 0.136$	T3 = 1.0	T1 = 9.94×10^9	T2 = 9.33×10^9
1396	$iC_3H_7OH(+M)$	=	$CH_3 + sC_2H_4OH(+M)$			
			high P limit	1.35×10^{24}	−2.27	89 960
			low P limit	2.85×10^{69}	−14.89	94 650
			Troe parameters: $a = 0.336$	T3 = 774.5	T1 = 9.68×10^9	T2 = 8.21×10^9
1397	$iC_3H_7OH(+M)$	=	$iC_3H_7 + OH(+M)$			
			high P limit	1.75×10^{22}	−1.75	96 320
			low P limit	3.92×10^{61}	−12.80	102 950
			Troe parameters: $a = 0.57$	T3 = 8.83×10^9	T1 = 754.8	T2 = 9.33×10^9
1398	$iC_3H_7OH + O_2$	=	$iC_3H_6OH + HO_2$	4.20×10^{13}	0.00	52 000
1399	$iC_3H_7OH + O_2$	=	$tC_3H_6OH + HO_2$	7.00×10^{12}	0.00	43 700
1400	$iC_3H_7OH + OH$	=	$iC_3H_6OH + H_2O$	1.05×10^{10}	0.97	1586
1401	$iC_3H_7OH + OH$	=	$tC_3H_6OH + H_2O$	2.99×10^{13}	−0.49	−235
1402	$iC_3H_7OH + H$	=	$iC_3H_6OH + H_2$	1.33×10^6	2.54	6756
1403	$iC_3H_7OH + H$	=	$tC_3H_6OH + H_2$	2.30×10^5	2.72	6260
1404	$iC_3H_7OH + O$	=	$iC_3H_6OH + OH$	1.96×10^6	2.43	4750
1405	$iC_3H_7OH + O$	=	$tC_3H_6OH + OH$	5.13×10^{11}	0.21	4890
1406	$iC_3H_7OH + CH_3$	=	$iC_3H_6OH + CH_4$	9.04×10^{-1}	3.65	7154
1407	$iC_3H_7OH + CH_3$	=	$tC_3H_6OH + CH_4$	2.39×10^{-4}	4.97	5710
1408	$iC_3H_7OH + CH_3O$	=	$iC_3H_6OH + CH_3OH$	3.00×10^{11}	0.00	7000
1409	$iC_3H_7OH + CH_3O$	=	$tC_3H_6OH + CH_3OH$	4.34×10^{11}	0.00	6460
1410	$iC_3H_7OH + HO_2$	=	$iC_3H_6OH + H_2O_2$	1.68×10^{13}	0.00	20 440
1411	$iC_3H_7OH + HO_2$	=	$tC_3H_6OH + H_2O_2$	2.80×10^{12}	0.00	14 860
1412	$iC_3H_7OH + CH_3O_2$	=	$iC_3H_6OH + CH_3O_2H$	1.68×10^{13}	0.00	20 440
1413	$iC_3H_7OH + CH_3O_2$	=	$tC_3H_6OH + CH_3O_2H$	2.80×10^{12}	0.00	14 860
1414	iC_3H_6OH	=	$C_3H_6 + OH$	6.41×10^{15}	−0.60	28 840
1415	iC_3H_6OH	=	$C_2H_3OH + CH_3$	2.69×10^9	1.32	29 480
1297	tC_3H_6OH	=	$CH_3COCH_3 + H$	8.98×10^{11}	0.27	32 990
1298	tC_3H_6OH	=	$iC_3H_5OH + H$	4.21×10^{10}	1.00	40 490

Table 3. Propanol Mixture Compositions, $p_5 = 1.0$ atm

mixture	equivalence ratio	fuel concentration	% O_2	% Ar
1	0.5	0.25% *n*-propanol	2.25	97.50
2	1.0	0.50% *n*-propanol	2.25	97.25
3	2.0	0.50% *n*-propanol	1.125	98.375
4	0.5	0.25% *iso*-propanol	2.275	97.475
5	1.0	0.50% *iso*-propanol	2.25	97.25
6	2.0	0.50% *iso*-propanol	1.125	98.375

maximum [CH] rise rates (for example +2−15% at highest temperatures), but they are very consistent over the conditions studied, including the parametric cases discussed in the next section. In addition, they agree fairly well with other τ definitions that have been used previously in the literature, including peak [CO] ($\tau_{CO,peak}$) or [OH] ($\tau_{OH,peak}$) concentrations, as well as backward extrapolation of peak [OH] rise rates. However, discrepancies are noted at higher temperatures and for rich mixtures where, for example, the differences between $\tau_{C_2H_xO,peak}$ and $\tau_{CO,peak}$ can be greater than ~80%. These differences, however, have only a small effect on the trends observed in the simulations, as discussed in the next section, including the activation energy which is altered by only 5% at $T = 2000$ K. A discussion of potential simulation/numerical errors associated with different definitions of τ at various conditions can be found in Goldsborough[70] (see Appendix A in that reference).

5. Results and Discussion

Ignition delay measurements for *n*- and *iso*-propanol were conducted at a variety of conditions including temperatures from approximately 1350 to 2000 K, equivalence ratios (ϕ) of 0.5, 1.0, and 2.0, and dilutions of $\chi_{O_2} = 1.13$ and 2.25% ($\chi_{fuel} = 0.5$ and 0.25%). (For this work ϕ is defined as the actual fuel-to-oxygen ratio relative to the stoichiometric fuel-to-oxygen ratio.) A summary of the fuel mixtures used is provided in Table 3. Compressed pressures near 1 atm were used in this study.

Figures 4 and 5 present the raw ignition delay times for *n*- and *iso*-propanol, respectively; a total of 157 points are shown for *n*-propanol and 121 for *iso*-propanol; the raw data is also provided as Supporting Information. Simulated ignition delay times at these conditions are shown. The times are plotted on logarithmic scale with respect to inverse temperature ($T^* = 10^4/T$). Experimental times have an error of about ±13%, and error in the temperature calculations is on the order of ±2.5%. A large number of experiments were performed across the temperature range in order to clarify the non-Arrhenius behavior (i.e. curvature in the log(τ) vs T^* diagram) that is observed in the mechanism (see the Ignition Time Correlation subsection for a discussion of this). There is significant scatter in the experimental times due to uncertainties, however the consistency between the points is quite good, more so at higher temperatures. At the lowest temperatures and the longest test times, for both the stoichiometric and rich mixtures, nonideal gas dynamic effects may influence the measured τ values. At the highest temperatures there may be errors associated with the use of endwall CH* emissions, which can result in excessively long τ values for the dilute conditions used, as discussed by Petersen.[71]

In Figure 4 the effects of *increasing* the oxygen concentration from 1.125% ($\phi = 2.0$) to 2.25% ($\phi = 1.0$), and of *decreasing* the fuel concentration from 0.5% ($\phi = 1.0$) to

(69) Lund, C. M. Chase, L., *HCT-A General Computer Program for Calculating Time-Dependent Phenomena Involving One-Dimensional Hydrodynamics, Detailed Chemical Kinetics and Transport, Rep. UCRL-52504*; Lawrence Livermore National Laboratory: 1995.

(70) Goldsborough, S. S. *Combust. Flame* **2009**, *156*, 1248–1262.

(71) Petersen, E. L. *Combust. Sci. Technol.* **2009**, *181*, 1123–1144.

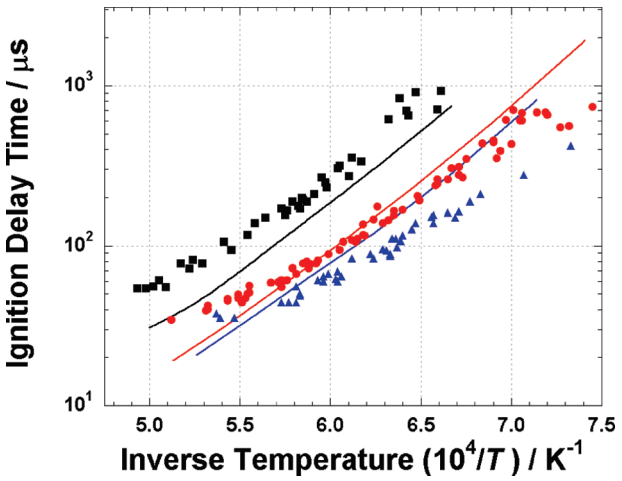

Figure 4. Ignition delay times for *n*-propanol in argon at 1 atm: ■ 0.5% fuel, 1.125% O_2, $\phi = 2.0$; ● 0.5% fuel, 2.25% O_2, $\phi = 1.0$; ▲ 0.25% fuel, 2.25% O_2, $\phi = 0.5$; lines, simulation.

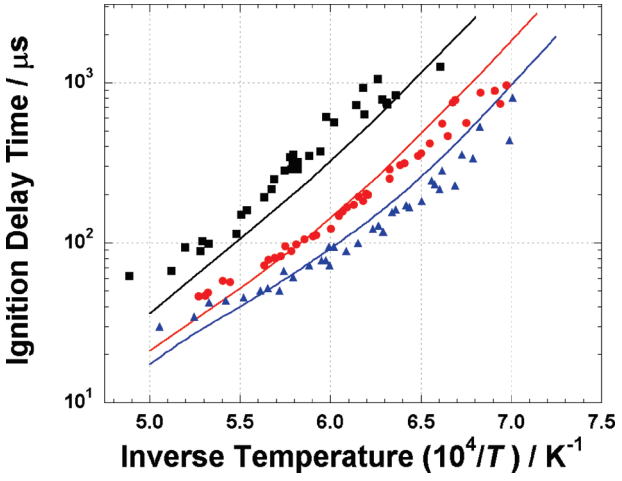

Figure 5. Ignition delay times for *iso*-propanol in argon at 1 atm: ■ 0.5% fuel, 1.125% O_2, $\phi = 2.0$; ● 0.5% fuel, 2.25% O_2, $\phi = 1.0$; ▲ 0.25% fuel, 2.275% O_2, $\phi = 0.5$; lines, simulation.

0.25% ($\phi = 0.5$) can be seen. Here we observe the high negative dependence of ignition time on oxygen which is observed at high temperatures ($1100 \leq T \leq 2000$ K) for almost all hydrocarbon and oxygenated hydrocarbon fuels, including n- and iso- butane. For *n*-propanol, the predicted ignition delays are in reasonable agreement with the experiment. At the lower temperatures for the fuel rich mixture ($T \sim 1500-1650$ K, $T^* \sim 6.7-6.0$ K^{-1}) the model predictions agree well with experimental results, but the model becomes too fast at higher temperatures. For the stoichiometric and lean mixtures on the other hand, the model predictions indicate slower reactivity at the lower temperatures and faster reactivity at higher temperatures, compared to experimentally measured delay times. It can therefore be inferred that there is a discrepancy between the experimental and model activation energies (often referred to as the slope on the log(τ) vs T^* diagram); this is discussed more in the Ignition Time Correlation subsection.

For *iso*-propanol (Figure 5) the model seems to be in slightly better overall agreement with the experiments. However, faster reactivity is predicted under fuel-rich conditions, while reasonable accuracy is achieved for the stoichiometric mixture, and the mechanism is slightly slow compared to the

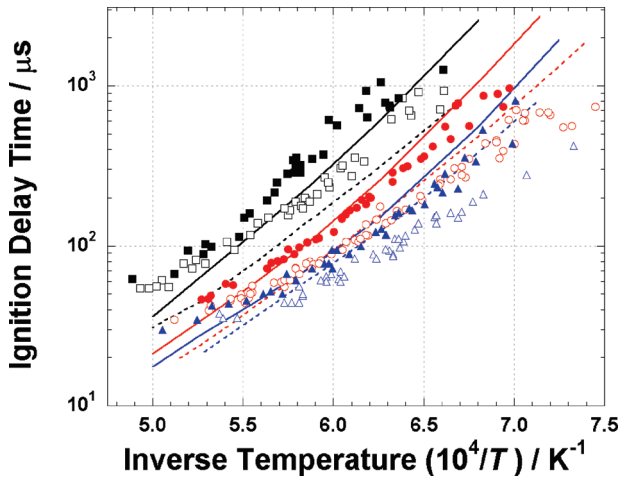

Figure 6. Comparative ignition delay times for both propanol isomers in argon at 1 atm: ■ 0.5% fuel, 1.125% O_2, $\phi = 2.0$; ● 0.5% fuel, 2.25% O_2, $\phi = 1.0$; ▲ 0.25% fuel, 2.275% O_2, $\phi = 0.5$, solid symbols *iso*-propanol, open symbols, *n*-propanol. Lines are simulated times, solid lines correspond to solid symbols, dashed lines to open symbols.

lean experiments, particularly at lower temperatures ($T < 1650$ K, $T^* > 6.0$ K^{-1}). As with the *n*-propanol, there appears to be a discrepancy between the experimental and model activation energies.

Figure 6 combines the results of Figures 4 and 5 so that the overall reactivity for the *n*-propanol and *iso*-propanol at rich, stoichiometric, and lean conditions can be compared. It is clear from the experimental results that ignition times for the *n*-propanol mixtures are faster than for *iso*-propanol in all cases. This behavior is captured by the propanol mechanism, and it is also seen in ST data between *n*- and *iso*-butane,[51,72−75] which is also discussed shortly. In order to better understand and interpret the trends seen in the experiments and the model a number of analyses are conducted; these include standard reaction flux and sensitivity analyses, as well as correlations of the ignition delay times. These are described next.

Flux Analysis. A flux analysis is performed for fuel oxidation under stoichiometric conditions at 1600 K, at 30% fuel consumption. This is a local analysis, meaning that it represents an instantaneous snapshot in time; cumulative or integrated effects are not captured with this approach. Figure 7 shows the main pathways for *n*-propanol consumption under these conditions, where the total ignition delay time is calculated to be 151.8 μs; 30% of the fuel is consumed by 15.3 μs. One can observe that at this time 29% of the fuel is consumed through unimolecular elimination, producing propene and water. Primary hydrogen atom abstraction from the fuel, mainly by H atoms and OH radicals, leads to the formation of the $3C_3H_6OH$ radical, which undergoes β-scission to yield ethylene and the hydroxyl-methyl radical. Both 1- and $2C_3H_6OH$ radicals are produced in about the

(72) Oehlschlaeger, M. A.; Davidson, D. F.; Herbon, J. T.; Hanson, R. K. *Int. J. Chem. Kinet.* **2004**, *36*, 67–78.
(73) Davidson, D. F.; Hanson, R. K. *Fundamental Kinetics Database Utilizing Shock Tube Measurements*; Stanford University: 2005.
(74) Lamnaouer, M.; Zinner, C.; Rotavera, B.; Petersen, E.; Bourque, G. *AIAA 2007−5658*, **2007**.
(75) Healy, D., Curran, H. J., Donato, N. S., Aul, C. J., Petersen, E. L., Zinner, C. M., Bourque, G., *n-Butane: ignition delay measurements at high pressure and detailed chemical kinetic simulations. Combust. Flame* Submitted Sept 2009, in review.

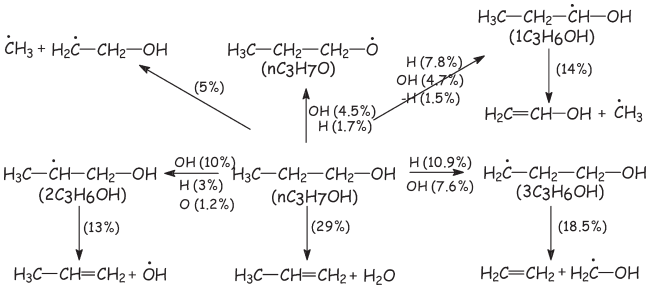

Figure 7. Main consumption pathway for 0.5% *n*-propanol, $\phi = 1.0$, $T = 1600$ K, $p_5 = 1$ atm at 30% fuel consumed.

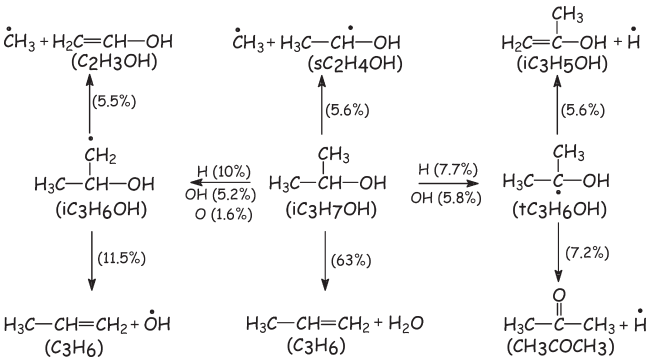

Figure 8. Main consumption pathway for 0.5% *iso*-propanol, $\phi = 1.0$, $T = 1600$ K, $p_5 = 1$ atm at 29% fuel consumed.

same amount, with the $1C_3H_6OH$ radical decomposing to produce vinyl alcohol (C_2H_3OH) and a methyl radical, while the $2C_3H_6OH$ radical decomposes to yield propene and an hydroxyl radical.

Figure 8 shows the main pathways for *iso*-propanol consumption under the same conditions as described for *n*-propanol, where the total ignition delay time in this case is calculated to be 254.9 μs; 29% of the fuel is consumed at 7.2 μs. For both *n*- and *iso*-propanol we have chosen to compare their reactivities at the point where the same amount of fuel has been consumed. In comparing the two isomers, we see that the time taken to consume 29% of the *iso*-propanol (7.2 μs) is significantly *shorter* than the time to consume 30% of the *n*-propanol (15.3 μs), even though the total ignition time of 254.9 μs for *iso*-propanol is significantly *longer* than the ignition delay of 151.8 μs for *n*-propanol. (This feature is slightly different than the low pressure, high χ_{O_2} MBMS flame results presented by Kasper et al.[39] where similar concentration (i.e., consumption) profiles were noted for *n*- and *iso*-propanol at stoichiometric fuel/O_2 ratios.) We believe that there are two reasons for the difference in predicted consumption/ignition behaviors; (i) significantly more *iso*-propanol undergoes unimolecular elimination to produce propene and water, which are two stable species (not radicals). The propene produced is relatively slow to oxidize as it undergoes hydrogen abstraction reactions, which mainly produce resonantly stabilized allyl radicals. (ii) In the case of *n*-propanol, higher concentrations of ethylene are produced and hydrogen atom abstraction reaction produce vinyl radicals, which react with molecular oxygen to produce relatively more reactive radicals.

Sensitivity Analysis. A sensitivity analysis is performed for *n*- and *iso*-propanol at the conditions of 0.5% fuel, $\phi = 1$ and p = 1 atm for temperatures of $T = 1481$, 1667, and 1905 K ($T^* = 6.75$, 6.00, and 0.525 K^{-1}, respectively). Normalized sensitivity

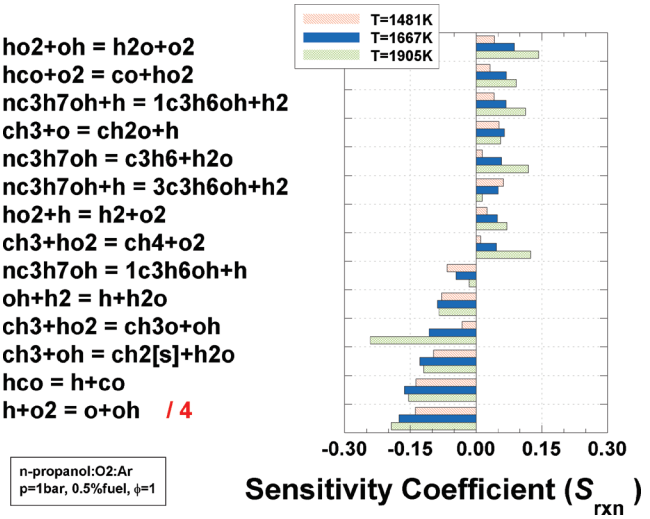

Figure 9. Sensitivity coefficients for 0.5% *n*-propanol, $\phi = 1.0$, $p_5 = 1$ atm, at $T = 1481$, 1667 and 1905 K; the most sensitive reactions at $T = 1667$ K are listed with coefficients shown at the other temperatures.

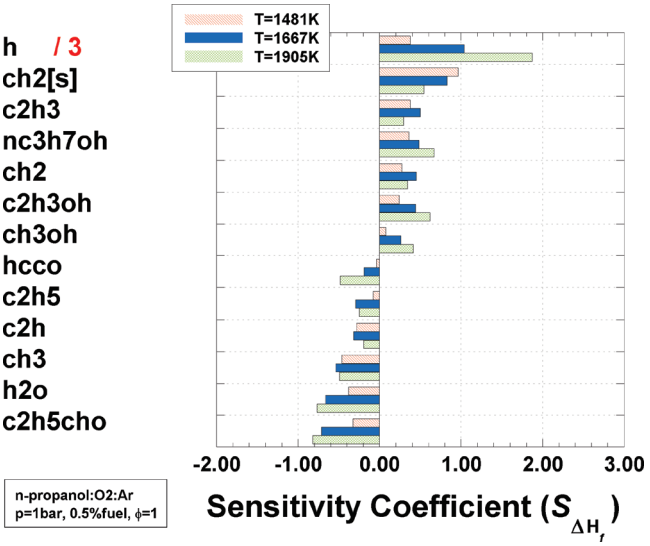

Figure 10. Sensitivity coefficients for 0.5% *n*-propanol, $\phi = 1.0$, $p_5 = 1$ atm, at $T = 1481$, 1667 and 1905 K; the most sensitive species at $T = 1667$ K are listed with coefficients shown at the other temperatures.

coefficients are listed in Figures 9 and 10 for *n*-propanol and in Figures 11 and 12 for *iso*-propanol, where the most sensitive reactions and species heats of formation are shown for the $T = 1667$ K condition with coefficients at the two other temperatures also indicated. The normalized sensitivity coefficients are defined as

$$S_{\mathrm{rxn}} = \frac{\partial \log \tau_k}{\partial \log k} = \frac{\partial \tau_k}{\partial k}\frac{k}{\tau_k} \approx \frac{\tau_{2k} - \tau_{0.5k}}{1.5\tau_{1k}} \quad (1)$$

$$S_{\Delta H_f} = \frac{\partial \log \tau_{\Delta H_f}}{\partial \log \Delta H_f} = \frac{\partial \tau_{\Delta H_f}}{\partial \Delta H_f}\frac{\Delta H_f}{\tau_{\Delta H_f}} \approx \frac{\tau_{1.05\Delta H_f} - \tau_{0.95\Delta H_f}}{0.1\tau_{1\Delta H_f}} \quad (2)$$

where these definitions take into account cumulative effects of the reactions and species on the overall ignition delay times.

These sensitivity results indicate, as should be expected, that lower hydrocarbon and hydrogen chemistry are very

important at the experimental conditions; initial fuel decomposition and a few succeeding steps are the most sensitive fuel chemistry seen here. In addition, many of the same reactions and species appear for both *n*- and *iso*-propanol. Propene decomposition is more important however for *iso*-propanol since, as seen with the flux analysis, more of the fuel decomposition proceeds through the water elimination reaction (1395) at these conditions.

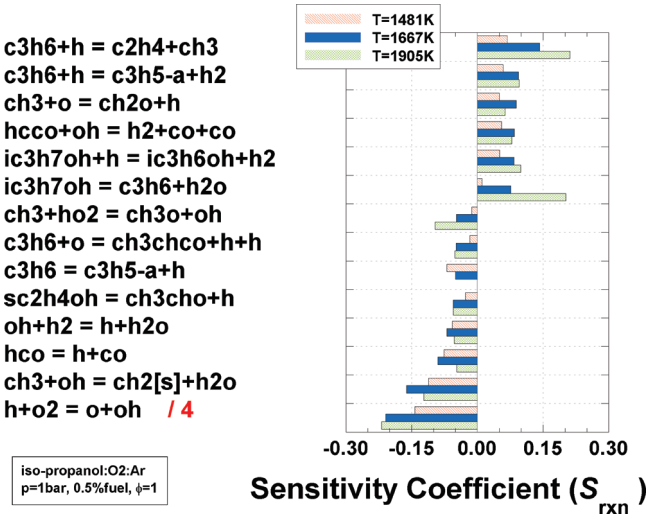

Figure 11. Sensitivity coefficients for 0.5% *iso*-propanol, $\phi = 1.0$, $p_5 = 1$ atm, at $T = 1481$, 1667, and 1905K; the most sensitive reactions at $T = 1667$ K are listed with coefficients shown at the other temperatures.

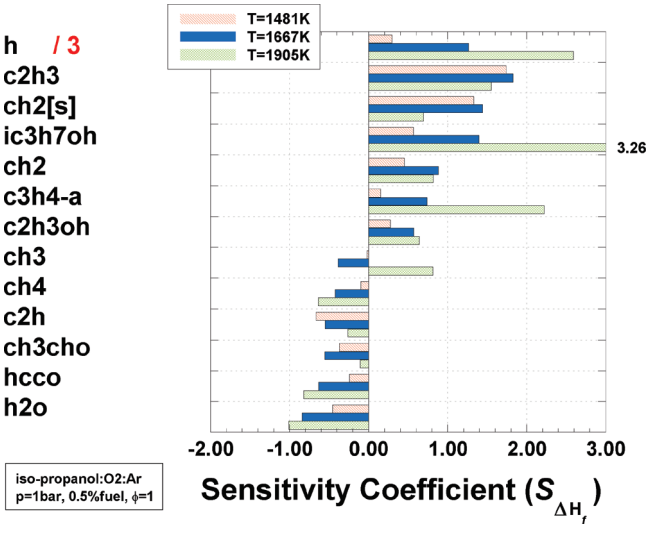

Figure 12. Sensitivity coefficients for 0.5% *iso*-propanol, $\phi = 1.0$, $p_5 = 1$ atm, at $T = 1481$, 1667, and 1905 K; the most sensitive species at $T = 1667$ K are listed with coefficients shown at the other temperatures.

Ignition Time Correlation. The measured ignition delay times and ignition times computed for all 278 experimental conditions are correlated to an Arrhenius-based, power law expression. This correlation form has been used successfully in many previous studies for straight, branched, and cyclic alkanes[51,70,76−78] in order to both normalize the data and to compare the functional dependencies that are apparent in the experiment and within kinetic models (e.g., see Chaos et al.[79]). This correlation can be expressed as

$$\tau = A\phi^{\alpha}p^{\beta}\chi_{O_2}^{\gamma} \times \exp(E_a/RT) \qquad (3)$$

where τ is ignition delay time (in μs), A is a scaling factor, ϕ is the equivalence ratio, p is pressure (atm), χ_{O_2} is the oxygen mole percent, E_a is activation energy (kcal/mol), R is the gas constant (kcal/(mol K)), and T is temperature (K). In this expression α, β, γ, and E_a represent the functionality of the reactive system with regard to ϕ, p, χ_{O_2}, and T, respectively; the interpretation of these parameters and how they reflect the underlying chemistry will be discussed shortly. Values for A, α, β, γ, and E_a are determined using a regression analysis of the experimental data, and of the simulated data points; these are listed in Table 4 where "exp" indicates experiment values and "mech" indicates values for the mechanism. Also listed in Table 4 are correlation constants for low pressure ST data for *n*-butane and *iso*-butane acquired at conditions similar to those used in this study.[51,72,73] The intent is to compare the overall reactivity of these structurally similar hydrocarbons as well as their functional dependencies.

Figure 13 presents correlated, or normalized, ignition delay times for *n*- and *iso*-propanol using a condition of $\phi = 1$, $p = 1$ atm, and $\chi_{O_2} = 2.25\%$ (0.5% fuel); both the normalized experimental points and the normalized simulated points are shown. Here, as with Figures 4−6, it can be seen that there is fairly good agreement between the experimental measurements and the mechanism predictions, however the difference in slopes between $(\tau_{exp})_{corr}$ and $(\tau_{sim})_{corr}$, identified in Figures 4 and 5, is again apparent. Also noticeable is the larger degree of scatter in the experimental times where standard deviations of ±16% and ±23% exist for the *n*- and *iso*-propanol, respectively, while standard deviations of ±5 and ±11% are noted for the simulated points, for *n*- and *iso*-propanol, respectively. Figure 14 illustrates normalized times for *n*- and *iso*-butane overlaid on the correlation results for propanol using the correlation parameters listed in Table 4. It can be seen that at these conditions the ignition delay times are very similar between these fuels, and that *n*-butane is more reactive than *iso*-butane.

The true functionality of the fuel/oxygen/diluent system is much more complex than the simple constants listed for eq 3; α, β, γ, and E_a are dependent not only on T^*, but also on ϕ, p, and χ_{O_2} as discussed in ref 70. Values for α, β, γ, and E_a extracted from regression analyses of data are necessarily weighted (i.e., skewed) toward the experimental conditions included. This is an important point that explains why different dependencies can be determined for the same fuel,

Table 4. Correlation Parameters for eq 3 for Propanol and Butane

fuel	A	α	β	γ	E_a (kcal mol^{-1})
n-propanol, exp	$2.37 \times 10^{-2} \pm 3 \times 10^{-3}$	0.66 ± 0.04	see text	-0.81 ± 0.07	29.86 ± 0.42
n-propanol, mech	$1.14 \times 10^{-3} \pm 5 \times 10^{-5}$	0.43 ± 0.01	see text	-0.74 ± 0.02	39.68 ± 0.12
iso-propanol, exp	$9.83 \times 10^{-3} \pm 2.3 \times 10^{-3}$	0.63 ± 0.07	see text	-0.94 ± 0.12	34.33 ± 0.77
iso-propanol, mech	$4.2 \times 10^{-4} \pm 5 \times 10^{-5}$	0.65 ± 0.03	see text	-0.53 ± 0.06	43.75 ± 0.36
n-butane[51,75]	$5.4 \times 10^{-4} \pm 3.7 \times 10^{-4}$	1.04 ± 0.1	-0.64 ± 0.07	-0.62 ± 0.06	41.34 ± 2.12
iso-butane[72,73]	$5.0 \times 10^{-5} \pm 2 \times 10^{-5}$	0.97 ± 0.05	-0.33 ± 0.03	-0.42 ± 0.02	48.51 ± 0.99

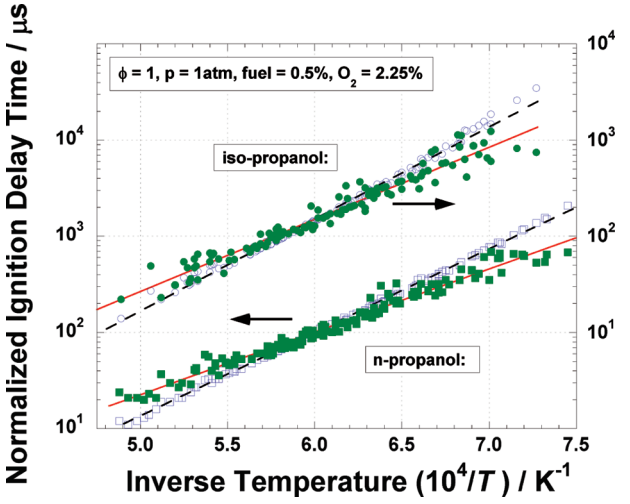

Figure 13. Normalized ignition delay times for both propanol isomers in argon at $\phi = 1$, $p = 1$ atm, and $\chi_{O_2} = 2.25\%$: ■ *n*-propanol, ● *iso*-propanol; solid symbols correspond to experiment, open symbols correspond to model. Lines are correlation equation, solid lines correspond to solid symbols, dashed lines to open symbols.

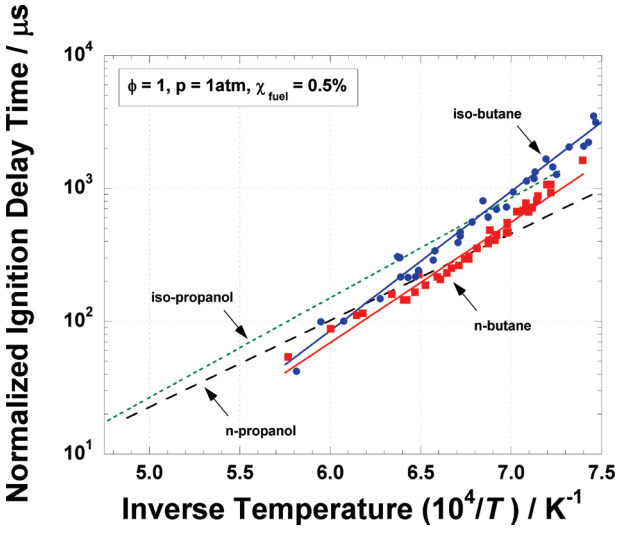

Figure 14. Comparison of normalized ignition delay times for *n*- and *iso*-butane with *n*- and *iso*-propanol in argon at $\phi = 1$, $p = 1$ atm, and $\chi_{fuel} = 0.5\%$, ■ *n*-butane, ● *iso*-butane. Lines are correlation equation, solid lines correspond to butane, dashed lines to propanol.

even at similar overall conditions. Although the true functionalities of the reactive system cannot be deduced from simple correlation constants where data sets sparsely populate the conditions of interest, the deduced values do provide an additional means of comparing experimental data and kinetic models, as has been done previously by Goldsborough[70] and Chaos et al.[79] These comparisons can provide an indication of agreement and deficiencies within a mechanism and could be used to improve a mechanism's performance.

(76) Petersen, E. L.; Davidson, D. F.; Hanson, R. K. *Combust. Flame* **1999**, *117*, 272–290.
(77) Qin, Z.; Yang, H.; Gardiner, W. C. *Combust. Flame* **2001**, *124*, 246–254.
(78) Daley, S. M.; Berkowitz, A. M.; Oehlschlaeger, M. A. *Int. J. Chem. Kinet.* **2008**, *40*, 624–634.
(79) Chaos, M.; Kazakov, A.; Zhao, Z.; Dryer, F. L. *Int. J. Chem. Kinet.* **2007**, *39*, 399–414.

In order to reveal the true functionality of the propanol/oxygen/argon system (and to provide a check for the correlation constants determined here) parametric simulations have been conducted with the new propanol mechanism covering a range of temperatures ($T = 1000-2000$ K with an interval of $\Delta T^* = 0.25\ K^{-1}$), equivalence ratios ($\phi = 0.5$, 1.0, and 2.0), pressures ($p = 1$, 4, and 8 atm), and oxygen concentrations ($\chi_{O_2} = 2$, 5, and 10%). Argon is used as the diluent gas in all of the calculations, and the ignition delay times are determined as described earlier. A total of 567 cases have been simulated for each of the two propanol isomers.

The functional dependencies from the parametric runs, α_{param}, β_{param}, and γ_{param}, are computed through the following expressions, where these are derived based on the power law form assumed for eq 3,

$$\alpha_{param} = \frac{\ln(\tau_2/\tau_1)}{\ln(\phi_2/\phi_1)};\ T_2 = T_1, p_2 = p_1, \chi_{O2_2} = \chi_{O2_1} \qquad (4)$$

$$\beta_{param} = \frac{\ln(\tau_2/\tau_1)}{\ln(p_2/p_1)};\ T_2 = T_1, \phi_2 = \phi_1, \chi_{O2_2} = \chi_{O2_1} \qquad (5)$$

$$\gamma_{param} = \frac{\ln(\tau_2/\tau_1)}{\ln(\chi_{O2_2}/\chi_{O2_1})};\ T_2 = T_1, p_2 = p_1, \phi_2 = \phi_1 \qquad (6)$$

The "param" notation here refers to the functions as determined from the parametric simulations. A determination of $E_{a,param}$ is not straightforward as it is with the α, β, and γ functions, due to the fact that an exponential function is used for E_a in eq 3; only changes in E_a from one temperature to another can be computed from the simulated ignition times, for example:

$$\ln\frac{\tau_2}{\tau_1} = \frac{E_{a_2}}{RT_2} - \frac{E_{a_1}}{RT_1};\ \phi_2 = \phi_1, p_2 = p_1, \chi_{O2_2} = \chi_{O2_1} \qquad (7)$$

However, for small steps in T^* this can be approximated as

$$E_a \approx \frac{R\ln(\tau_2/\tau_1)}{(1/T_2 - 1/T_1)};\ \phi_2 = \phi_1, p_2 = p_1, \chi_{O2_2} = \chi_{O2_1} \qquad (8)$$

Figures 15–17 present the functional dependency terms α, β, and γ for the parametric simulations along with the correlation values listed in Table 4. Figure 15 shows the dependency of ignition on equivalence ratio. It is first noted in this figure that the $\alpha_{corr,sim}$ values are close to the α_{param} trend lines for applicable conditions, that is, $p = 1$ atm, $\chi_{O_2} = 2\%$ (the trend lines for this are thin blue traces). This agreement is clearer in the case of *n*-propanol due to the large spread in α_{param} at various dilution levels and pressures. The agreement indicates a degree of confidence in the regression analysis results; however, due to the complexity in α, β, and γ, larger discrepancies could be expected over wider experimental conditions. Also noted in this figure and in Table 4, is that $\alpha_{corr,exp}$ and $\alpha_{corr,sim}$ are fairly close (for both fuels) indicating that the trends in ignition timing with increasing/decreasing ϕ are similar between the experiments and the kinetic mechanism. Agreement between the *iso*-propanol values is slightly better than for *n*-propanol. It is unclear however, how the mechanism will compare with experimental data far from the experimental conditions used here, for example, at the high O_2 concentrations used in ref 39. The values of $\alpha_{corr,exp}$ for butane are slightly greater than for those for the propanol isomers.

Another interesting feature can also be seen when comparing the *n*- and *iso*-propanol functionalities in Figure 15.

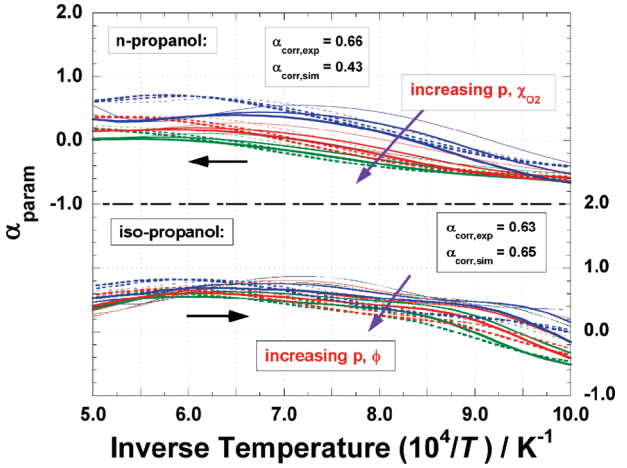

Figure 15. Equivalence ratio dependency, α, as a function of T^* for both propanol isomers. The data covers $T^* = 5.0-7.5$ while parametric values cover $T^* = 5.0-10.0$. Blue lines are $\chi_{O_2} = 2\%$, red are $\chi_{O_2} = 5\%$, green are $\chi_{O_2} = 10\%$; thinnest lines are $p = 1$ atm, thicker lines are $p = 4$ atm, thickest lines are $p = 8$ atm; solid lines are $\phi_2 = 0.5$, dashed lines are $\phi_2 = 2.0$. Trends with increasing p, ϕ, and χ_{O_2} are highlighted.

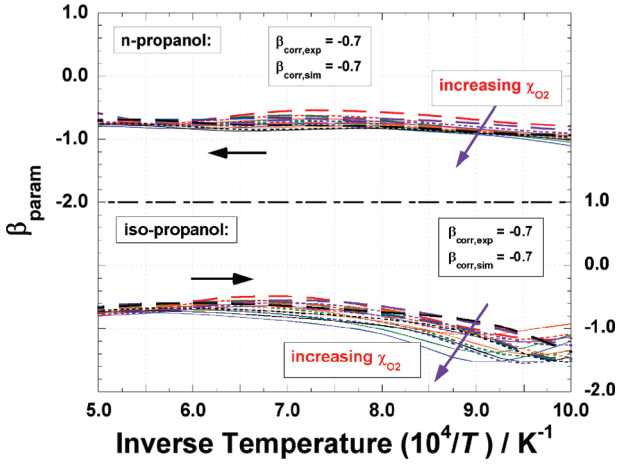

Figure 16. Pressure dependency, β, as a function of T^* for both propanol isomers. The data covers $T^* = 5.0-7.5$, and parametric values cover $T^* = 5.0-10.0$. Red lines are $\phi = 0.5$, $p_2 = 8$ atm; green are $\phi = 1.0$, $p_2 = 8$ atm; blue are $\phi = 2.0$, $p_2 = 8$ atm; purple are $\phi = 0.5$, $p_2 = 1$ atm; yellow are $\phi = 1.0$, $p_2 = 1$ atm; black are $\phi = 2.0$, $p_2 = 1$ atm. Solid lines are $\chi_{O_2} = 10\%$, short dashed lines are $\chi_{O_2} = 5\%$, long dashed lines are $\chi_{O_2} = 2\%$. Trends with increasing χ_{O_2} are highlighted; no trends with p or ϕ are noted.

In high temperature regimes, that is, $T > 1150$ K, it has been noted for many alkanes (including larger ones such as *n*-heptane, *iso*-octane) that rich mixtures are less reactive than lean ones due to the increasing competition with the important chain branching reaction $H+O_2 = O+OH$ as the relative fuel concentration increases.[42] Values for α at high temperature have been reported as greater than zero across a range of conditions, meaning that ignition delay times are longer for rich mixtures; this is the behavior seen for *iso*-propanol in the parametric simulations conducted. For *n*-propanol however, at higher charge concentrations the values of α_{param} are seen to *decrease* to values such that rich mixtures are predicted to ignite just as fast as, or even faster than stoichiometric ones. From an initial observation of the mechanism this appears to be due to the increasing importance of formyl radical chemistry at high fuel/oxygen

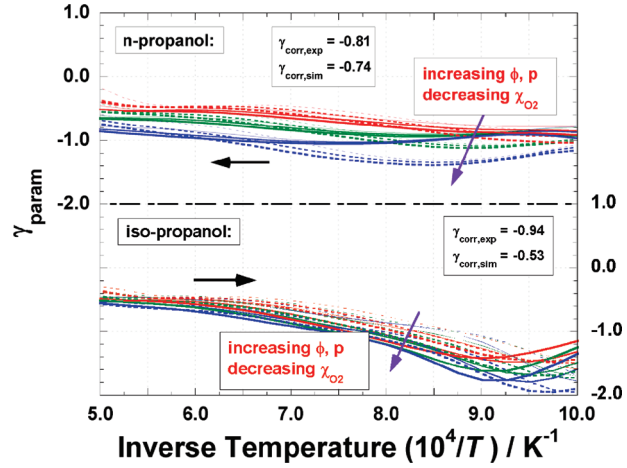

Figure 17. Oxygen (i.e., dilution) dependency, γ, as a function of T^* for both propanol isomers. The data covers $T^* = 5.0-7.5$, and parametric values cover $T^* = 5.0-10.0$. Red lines are $\phi = 0.5$, green are $\phi = 1.0$, blue are $\phi = 2.0$; thinnest lines are $p = 1$ atm, thicker lines are $p = 4$ atm, thickest lines are $p = 8$ atm; solid lines are $\chi_{O_2} = 10\%$, dashed lines are $\chi_{O_2} = 2\%$. Trends with increasing p and ϕ, and decreasing χ_{O_2} are highlighted.

concentrations, particularly through HCO = H + CO and $HCO + O_2 = CO + HO_2$.

This functionality (i.e., $\alpha \sim 0$) also seems to be exhibited in the experimental MBMS data of Kasper et al.[39] and in the corrected MBMS data of Li et al.[38,40] In their low pressure burner experiments with very high O_2 concentration ($\chi_{O_2} \sim 50\%$) both groups found that at their leanest conditions, $\phi = 1$ for Kasper et al.[39] and $\phi = 0.5$ for Li et al.,[38] there was no noticeable difference in the consumption rates for *n*- and *iso*-propanol, meaning that the fuel concentration profiles above the burners were almost identical for the two isomers. However, as the equivalence ratio was increased, to $\phi = 2$ in Kasper et al.[39] and to $\phi = 2$ in Li et al.,[38,40] the consumption rate of *n*-propanol became greater than *iso*-propanol such that both research groups observed an earlier drop in *n*-propanol concentration above their burners. This indicates a change in relative reactivities between the isomers in their experiments as the equivalence ratio is altered; this observation appears to confirm the behavior seen in α_{param} in Figure 15.

Another indication that the predicted functionality for α_{param} is valid can be found in the ST data for *n*- and *iso*-butane.[51,72−75] In these data sets high dilution mixtures ($\chi_{O_2} \sim 2\%$) exhibit values of α which are positive for both fuels[51,72,73] (see Table 4), and high charge strength (i.e., undiluted) mixtures ($\chi_{O2} \sim 21\%$) have values of α that are positive for *iso*-butane, but near zero for *n*-butane.[74,75] Additional insight into this feature is beyond the scope of this paper.

Figure 16 next displays the dependency of ignition on pressure as determined from the parametric runs. Except at the highest charge concentrations for *iso*-propanol, there is very little variation in β_{param} with temperature, or with any of the other parameters. For the correlation fits therefore constant values near −0.7 were selected for both propanol isomers, since only pressures of 1 atm were used in the experiments. This value for $\beta_{corr,exp}$ was selected in order to fall near the parametrically computed values for the experimental ST conditions. Pressure effects at these conditions are generally attributable to changes in molecular mean free paths, meaning that higher pressure increases the relative reactivity due to increased collisions.

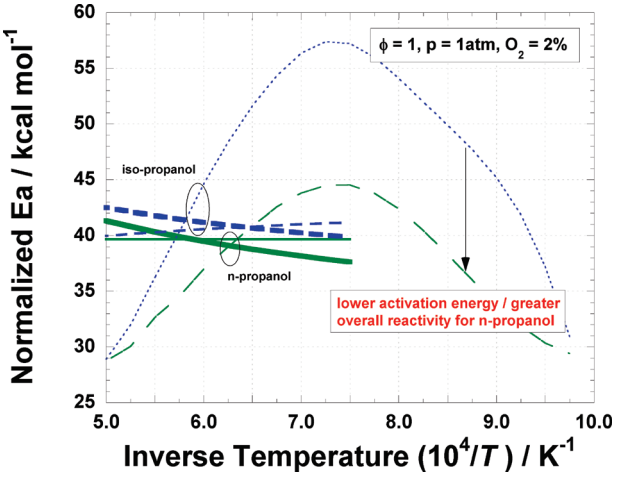

Figure 18. Normalized activation energies for both propanol isomers in argon at $\phi = 1.0$, $p = 1$ atm, and $\chi_{O_2} = 2\%$, *n*-propanol (solid green line), *iso*-propanol (dashed blue line), heavy bold lines correspond to experimental correlation, thick lines to correlation of simulated points, thin lines to parametric simulations.

Figure 17 next illustrates the dependency functions for χ_{O_2}, or dilution, for *n*- and *iso*-propanol. Here we see a high negative dependence of ignition on O_2 concentration, as was noted in Figures 4−6, where important reactions at the experimental conditions include $H + O_2 = O + OH$, $CH_3 + HO_2 = CH_3O + OH$, and $HCO = H + CO$. In addition, we note that the differences between the correlated experimental and simulation values, especially for *iso*-propanol, are greater than those seen with the α functions. This discrepancy deserves further investigation and may indicate that the dilution functionality within the mechanism needs improvement. Additional experiments at various dilution levels could provide insight regarding these discrepancies. Values of $\gamma_{corr,exp}$ for *n*- and *iso*-butane are slightly smaller in magnitude than for *n*- and *iso*-propanol, but they are also negative.

Finally, Figure 18 is presented to compare the activation energies seen in the experiments with those observed in the kinetic model. Parametric values are determined using eq 8, and the correlated values are normalized in order to account for differences in the scaling factor used in eq 3. The normalization is accomplished by $E_{a,norm} = E_a + \ln(A/A')/RT$ where A' is a reference, or normalizing value. For Figure 18, A' is selected as 1.14×10^{-3}, which is the value for the fit of the simulated data points for *n*-propanol (see Table 4). In Figure 18 a number of trends can be seen. First, for both the experiments and the simulation the straight-chain alcohol has a lower activation energy and thus higher reactivity at the experimental conditions. This should be expected based on the discussion regarding Figures 5 and 6, where it is seen that unimolecular decomposition of the branched fuel molecule proceeds to a greater extent through the dehydration reaction. This tends to result in slower chain branching and ignition since the propene and water produced are not very reactive. This difference in reactivity has also been noted in ST ignition experiments with the normal and branched isomers of butanol.[31] Normalized values of E_a for *n*- and *iso*-butane are ∼39.2 and ∼40.2 kcal/mol, respectively, indicating similar activation energies and ignition delay times to propanol, as well as faster reactivity for the straight-chain hydrocarbon relative to the branched molecule

In Figure 18 it can be seen that there is a large discrepancy between $E_{a,corr,sim}$ and $E_{a,param}$ for both isomers with the parametric values varying significantly with temperature; this variation yields the non-Arrhenius behavior seen in the log τ_{mech} vs T^* plots. At fuel-rich and fuel-lean conditions (not shown here), $E_{a,param}$ exhibits similar profiles as the stoichiometric case, but with shifted maxima. $E_{a,corr}$ is assumed to be a constant value for eq 3, and the value deduced from the regression analysis of the data is weighted to cover a range of ϕ and T^* in the experiments. The correlated values, however, fall fairly close to the values determined from the parametric runs, which provides a degree of confidence in the regression analysis used. There are visible differences between $E_{a,corr,sim}$ and $E_{a,corr,exp}$ for both propanol isomers, indicating discrepancies between the kinetic model and the experimental ST data. These trends follow the behavior seen in the ignition delay times (Figures 4−6) where the mechanism indicates more reactivity (i.e., lower E_a/shorter τ) at the highest temperatures, and less reactivity (i.e., higher E_a/longer τ) at the lowest temperatures. The discrepancies seen in $E_{a,corr}$ could be due to the experimental issues discussed previously, as well as issues associated with the kinetic model, which need further investigation.

6. Summary and Conclusions

Ignition delay times for the two isomers of propanol (*n*-propanol and *iso*-propanol) have been measured in a shock tube using dilute mixtures of propanol, oxygen, and argon. Reflected temperatures ranging from approximately 1350 to 2000 K and a pressure of 1 atm have been used with equivalence ratios of 0.5, 1.0, and 2.0. Pressure measurements and CH* emissions were utilized to determine ignition delay times. A kinetic model has been developed to describe the decomposition and ignition pathways of both isomers in this temperature range. It is based on previously validated C3- chemistry with submechanisms added for the propanol isomers.

The experimental and simulated ignition results are analyzed using standard reaction flux and sensitivity analyses as well as correlations of the experimental and simulated ignition delay times. Correlated dependencies for ϕ, χ_{O_2}, and T in the experiment are compared to correlated dependencies seen in the simulated data points, and to dependencies determined through parametric simulations with the detailed kinetic mechanism. The overall trends in the data are captured fairly well by the mechanism, which include a greater level of reactivity for the *n*-propanol mixtures relative to *iso*-propanol. On the basis of the model results this is due to the fact that the branched fuel molecule proceeds to a greater extent through the dehydration reaction at the experimental conditions which results in slower chain branching since the propene and water that are produced are not very reactive. Ignition delay times are sensitive to lower hydrocarbon and hydrogen chemistry as well as a few fuel decomposition steps. The ϕ dependency (α) indicates fairly good agreement between the experiment and the model, whereas the dependencies of χ_{O_2} (γ) and T (Ea) need further investigation.

Acknowledgment. Funding for this work has been provided by the US National Science Foundation (CBET-0521602), Science Foundation Ireland (CHEF845), and Marquette University. Their support is gratefully acknowledged.

Supporting Information Available: Experimental ignition delay times are listed in Tables SI1 and SI2. This information is available free of charge via the Internet at http://pubs.acs.org/.